Liquid Nanostripes

Antonio Checco, Oleg Gang, and Benjamin M. Ocko*

Condensed Matter Physics and Materials Science Department, Brookhaven National Laboratory, Upton, New York 11973, USA

(Received 12 October 2005; published 9 February 2006)

Equilibrium wetting of ethanol, a volatile liquid, onto chemically patterned nanostripes has been investigated using noncontact atomic force microscopy (AFM). The chemical patterns, generated by a conducting AFM tip, are composed of COOH terminated ''wetting'' regions and CH_3 terminated ''nonwetting'' regions. Controlled amounts of ethanol, from the vapor phase, condense on the COOH stripes and their shape is imaged *in situ* versus their width ($70 < w < 300$ nm). The measured profile shapes at saturation and their $w^{1/2}$ height dependence are well described by density functional theory with dispersive, nonretarded potentials.

DOI: 10.1103/PhysRevLett.96.056104 PACS numbers: 68.08.Bc, 68.15.+e, 68.37.Ps

The equilibrium wetting of macroscopic droplets on a homogeneous solid substrate is well described by the classical theory of capillarity introduced two centuries ago by Young and Laplace [1]. The molecular interactions which give rise to thermodynamic quantities, such as bulk and surface energies, are also responsible for new phenomena at nanolength scales including the predicted deviation in the shape of drops [2,3] as compared to classical capillary theory. In this Letter we make use of chemically nanopatterned surfaces as templates for the condensation of nanometer-sized liquid drops. The patterns are composed of parallel, wettable nanostripes surrounded by an otherwise nonwettable surface. Although the wetting on a similar pattern with micrometer dimension is well described within classical capillary theory [4], at present there are only theoretical predictions concerning the wetting of ''nanostriped'' surfaces. In particular, it has been predicted that the liquid adsorption on the stripes scales with the stripe width according to a simple power law [3] at the liquid-vapor coexistence. We have used atomic force microscopy (AFM) to image volatile ethanol nanodrops, condensed onto the nanostripes, under equilibrium conditions with its vapor. Our results are in good agreement with the theory at saturation.

The fabrication of the chemical patterns and the wetting experiments were conducted with a Pico Plus (Molecular Imaging) AFM which is contained in an environmental chamber compatible with saturated vapors of water and ethanol. To control the ethanol adsorption, the temperature offset ΔT between the sample and the liquid reservoir (25 °C) was adjusted over a wide range (±15 °C) with an accuracy of 0.01 °C. The chemical patterns were prepared on Silicon (100) wafers (p doped, resistivity $<100\ \Omega$ cm) passivated with a hydrophobic monolayer of octadecylthricholorsilane molecules (OTS) according to standard procedures [5]. This self-assembled monolayer (SAM) is composed of all trans-hydrocarbon chains terminated by methyl groups. The well-packed SAMs exhibited a water contact angle of 110°, an x-ray reflectivity determined 24 Å thickness and a 3 Å roughness, consistent with literature values [6]. AFM studies also confirmed the presence of a nearly defect free, well-packed SAM.

The OTS terminated wafers were chemically nanopatterned using local oxidation nanolithography [5]. Here a metallic, biased, AFM tip contained in a humid environment is used to electrochemically oxidize the terminal methyl group to a hydrophilic carboxylic acid group. By changing the bias and humidity we were able to write stripes of varying widths [7]. As discussed below, the carboxylic acid and methyl terminated regions have very different wetting properties. Figs. 1(a) and 1(b) show images of the ''chemical lines'' obtained with AFM using two different imaging modes. Whereas the topography mode image (a) exhibits weak topographical contrast, the friction mode image (b) reveals differences in the chemical nature of the surface [8]. The topographical image (a) proves that the chemical patterning has a minimal effect (<3 Å) on the nanolandscape [7,9]. The writing line width (b) appears to be limited by the tip size, typically 30–40 nm in our case (MikroMasch, CSC17).

Wetting studies on chemical nanostripes were carried out using the AFM described above where the environ-

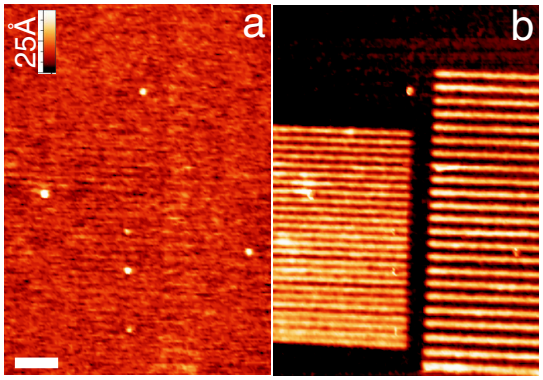

FIG. 1 (color online). (a) AFM contact mode image of an OTS substrate chemically patterned with hydrophilic stripes using local oxidation nanolithography. (b) Corresponding AFM friction force image showing the position of the hydrophilic stripes (white lines). The lateral-scale bar is 300 nm.

mental cell has been saturated with ethanol vapors. Ethanol was chosen as the wetting fluid since it has a reasonably high vapor pressure and it completely wets the acid terminated nanostripes. In addition, the ethanol does not wet the lower energy OTS surface as evidenced by the 30° contact angle of macroscopic (millimeter-sized) drops on methyl terminated surfaces. The morphology of the condensed ethanol profiles was investigated with amplitude modulation AFM (AM-AFM) in the noncontact regime [10]. To operate in this regime, which only involves long-range, attractive tip and sample interactions, the cantilever was modulated with a small amplitude (1–10 nm) at a fixed frequency about 100 Hz above the fundamental resonance. We have shown [7] that the liquid profiles can be reliably recorded only in the noncontact regime. Previously the noncontact AM-AFM [7,11], as well as other imaging modes [12–14], have been successfully used to image liquid micro- and nanodroplets.

Figures 2(a)–2(c) show the apparent AFM height images of condensed ethanol on five parallel nanostripes of width w ranging from 70 to 300 nm. In the following, the under-saturated, saturated, and over-saturated regimes correspond to ΔT being positive, zero, or negative, respectively. Each picture corresponds to a fixed ΔT equal to (a) 3 °C, (b) 0 °C, and (c) −10 °C. Corresponding transverse profile shapes are shown in Fig. 2(d). By using nanostripes of different widths it is possible to study the dependence of the liquid profiles on w for exactly the same ΔT. For $\Delta T = 3$ °C, a thin, relatively uniform liquid film (~1 nm) only a few molecules thick covers the stripes [Figs. 2(a) and 2(d)]. Close to saturation ($\Delta T \cong 0$) the liquid profile appears slightly curved and the maximum liquid thickness on the stripe increases monotonically with the stripe's width [Figs. 2(b) and 2(d)]. For the over-saturated case [$\Delta T = -10$ °C, Figs. 2(c) and 2(d)] the maximum thickness has increased further and the liquid profiles closely resemble that of cylindrical shaped, semi-infinite drops.

These images clearly demonstrate that the ethanol completely wets the COOH terminated lines and that it stays confined to these regions without "spillover" onto the methyl terminated surface. Further, the liquid stripes are stable and do not break up into a line of nanodrops. From profiles such as those shown in Fig. 2 we have obtained the maximum liquid thickness on the stripes, h, as a function of w for several ΔT. Figure 3 summarizes the h dependence versus w on a log-log plot for a series of temperatures. In the under-saturated case there is a weak dependence of h on w, especially at large w. At saturation (coexistence) the data appear to follow a power law dependence, $h \sim w^{\alpha}$ where $\alpha = 0.5 \pm 0.1$. In contrast, for over-saturated conditions the scaling behavior does not follow a simple power law over the entire range. However, for large w, h is consistent with a power law with $\alpha \simeq 2$.

The adsorption behavior on the chemical pattern, as well as the detailed morphology of the liquid nanostripes, depends on the specifics of the liquid-liquid and liquid-substrate interactions. For $\Delta T = 3$ °C, when the liquid film is molecularly thin, the short-range hydrogen-bond interactions between the ethanol molecules and the carboxylic surface dominate. On the other hand, long-range

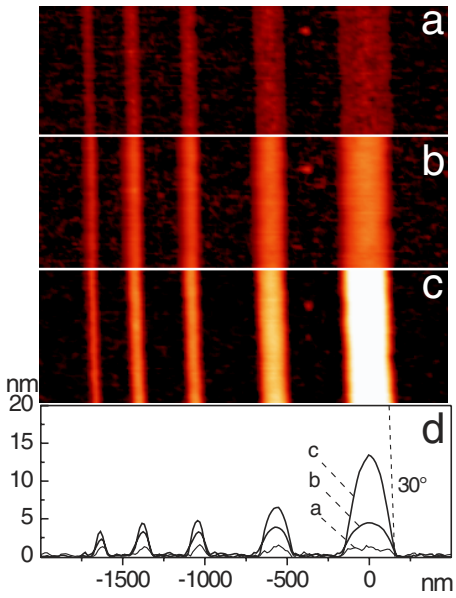

FIG. 2 (color online). Noncontact AM-AFM images (topography) show the condensation patterns of ethanol onto hydrophilic nanostripes for ΔT equal to (a) 3 °C, (b) 0° C, and (c) −10 °C. In (d) the corresponding cross-sectional liquid profiles are shown where the dashed line represents the contact angle of ethanol on OTS.

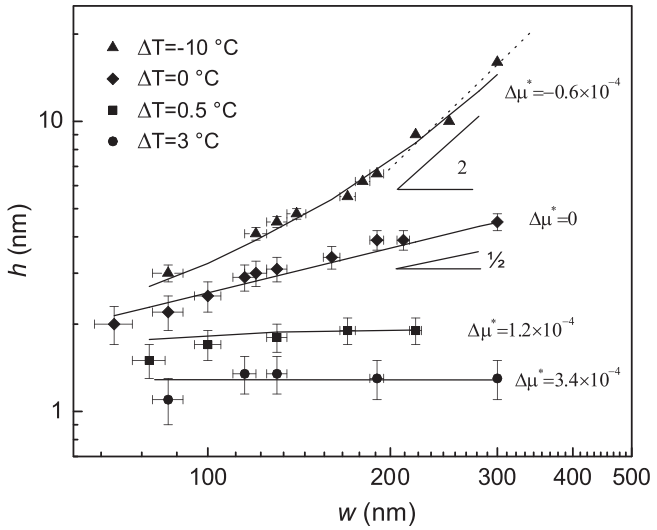

FIG. 3. The maximum liquid thickness h as a function of the stripe width w for a given ΔT. Solid lines are values calculated theoretically with $A = 2.3 \times 10^{-22}$ J and $\Delta\mu^*$ as given in the figure.

forces become relevant when the film is thicker than a few molecular layers. In the case of ethanol, a short chain alcohol, the long-range interactions can be adequately described by purely dispersive potentials [15]. This makes it possible to describe the shape of the liquid nanostripes that are thicker than a few molecular lengths by using microscopic density functional theory (DFT) [3]. In the following, we compare our experimental data to these theoretical predictions.

The profile of a liquid nanostripe is obtained by solving the "augmented Young equation" [16]:

$$\gamma \frac{l''(x)}{\sqrt{(1+l'^2(x))^3}} = \rho\Delta\mu + \frac{\partial\omega_{\mathrm{CS}}(x,l(x))}{\partial l}. \qquad (1)$$

This expression relates the local interface curvature (left hand side) to the chemical potential difference between the vapor and its liquid phases and the partial derivative of the "effective interface potential," $\omega_{\mathrm{CS}}(x, l(x))$, often referred to as the disjoining pressure. $\omega_{\mathrm{CS}}(x, l(x))$ is the excess free energy of a liquid film, thickness $l(x)$ at the coordinate x in the plane of the substrate and perpendicular to the stripe direction [3]. Although this equation only holds when the curvature of the liquid interface is small (the so called "local approximation"), in practice it gives results very similar to the more rigorous approach accounting for curvature effects [17]. In the framework of DFT, ω_{CS} can be expressed in term of $\omega_{\pm}(l)$, the effective potential of an ethanol film of thickness l covering the carboxylic (+) or methyl (−) surface, respectively. The latter potentials take the following functional form [17]:

$$\omega_{\pm}(l) = \rho\sigma^3\left\{-\frac{32}{9}\frac{\epsilon}{\sigma^2}\left[1+\frac{l-d_w^{\pm}}{\sigma}\arctan\left(\frac{l-d_w^{\pm}}{\sigma}\right)-\pi/2\right] + \frac{u_3^{\pm}}{2l^2}+\frac{u_4^{\pm}}{3l^3}-\frac{u_9^{\pm}}{8l^8}\right\}, \qquad (2)$$

where ρ is the ethanol number density, and $\epsilon = 5\times10^{-22}$ J and $\sigma = 0.2$ nm correspond, respectively, to the energy and length constants of the Lennard-Jones (LJ) liquid-liquid potential. ϵ and σ were selected to be consistent with the macroscopic ethanol surface tension $\gamma = 0.023\ \mathrm{J/m^2}$. The term in the square brackets takes into account the liquid-liquid interactions in a film of thickness $l - d_w^{\pm}$ where $d_w^{\pm}$ fixes an excluded volume due to hard-core liquid-solid repulsion. The other terms derive from a pairwise sum over the LJ solid-liquid interactions (minus higher order terms). In particular, we have chosen $u_3^{\pm} = 3.3\epsilon$, $u_4^{+} = 5\epsilon\sigma$, $u_4^{-} = 1.7\epsilon\sigma$, $u_9^{+} = 0.9\epsilon\sigma^6$, $u_9^{-} = 0.2\epsilon\sigma^6$, and $d_w^{\pm} = 0.15$ nm.

These parameters were adjusted such that the effective potentials describe adequately the wetting of ethanol on the carboxylic and methyl surfaces, respectively. As shown in the inset in Fig. 4, ω_- has a local negative minimum, equal to the spreading parameter $S = \gamma(\cos\theta - 1) = -3.1\times10^{-3}\ \mathrm{J/m^2}$ of ethanol on the methyl surface as we have measured experimentally. ω_+ describes instead the complete wetting ($S = 0$) of ethanol on the carboxylic stripe. As stated above, in the case of thin films ($l \sim \sigma$), where the liquid density is expected to be layered [15], the above implementation of DFT is not quantitatively reliable and a more rigorous approach is required. Nevertheless, since we have only measured films thicker than 1.3 nm the effects of molecular layering and short-range hydrogen bonding were not included. In the limit of thick liquid films, it can be shown that the potential is independent of the surfaces' outermost functional groups [15]. For this reason both potentials have the same long-range tail $\omega_{\pm}(l \gg \sigma) = A/l^2$ where $A = \frac{1}{2}\rho(u_3\sigma^3 - \frac{64}{27}\rho\epsilon\sigma^6)$ is the Hamaker constant.

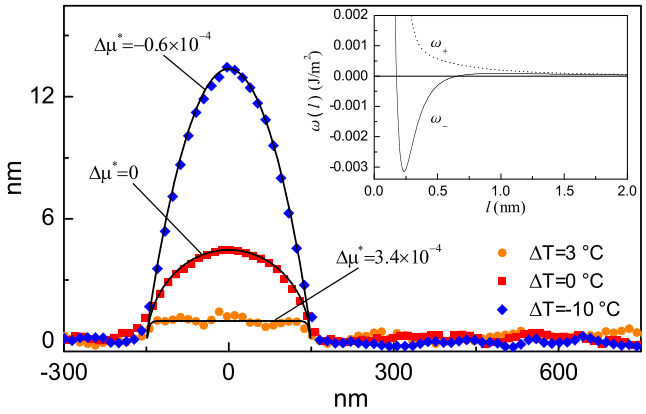

FIG. 4 (color online). Noncontact AM-AFM height profiles (dots) of a liquid film on a wettable stripe. Solid lines represent theoretical profiles calculated assuming $A = 2.3\times10^{-22}$ J and $\Delta\mu$ as adjustable parameter. The inset shows the shape of the potentials, $\omega_{\pm}(l)$.

Calculated profiles of the liquid nanostripes were obtained by solving numerically Eq. (1) for a given value of A and several different values of w and $\Delta\mu^* = \Delta\mu/kT$. In Fig. 4 we compare experimental and calculated profiles for $w = 300$ nm and several values of ΔT. The value of the Hamaker constant, $A = 2.3\times10^{-22}$ J, was chosen such that the maximum film thickness at saturation (middle curve) is equal to our experimentally determined drop height. A is close to the value estimated by considering that the solid substrate is layered and that the Hamaker constant of the silicon, OTS, and ethanol are respectively $A_{\mathrm{Si}} = 6\times10^{-21}$ J [15], $A_{\mathrm{OTS}} = 2\times10^{-21}$ J [18], and $A_{\mathrm{eth}} = 1\times10^{-21}$ J [15]. As shown in Fig. 4, the computed liquid shapes provide an excellent description of the overall experimental profiles except near the contact line. Here the experimental profiles appear broadened by about $\sim$10 nm, a value close to the AFM tip radius. The profiles corresponding to the under-saturated and over-saturated regimes are well described using $\Delta\mu^*$ equal to 3.4×10^{-4} and -0.6×10^{-4}, respectively. However, the $\Delta\mu$ calculated from ΔT, according to the expected bulk relation $\Delta\mu = q\Delta T/T$ where q is the latent heat of vaporiza-

tion per molecule of ethanol, is ~2 orders of magnitude larger than the fitted value. Presently we do not have an explanation for this discrepancy. In the thin liquid film regime at $\Delta T = 3\,^{\circ}\mathrm{C}$ the liquid interface is not flat but it exhibits a roughness close to that of the dry substrate. The roughness features are reproducible indicating that the AFM pictures are not due to instrumental noise or liquid surface fluctuations. This suggests that the surface of ultrathin liquid films exhibits "correlated roughness" [19] which results from the static topography or chemical features of the underlying surface [20]. At saturation the experimental profile is semielliptical [3] while in the over-saturated regime ($\Delta T = -10\,^{\circ}\mathrm{C}$) the shape is well approximated by a circle with an apparent 10° contact angle at the stripe boundary. For all ΔT investigated here we found that, as expected, the liquid does not spill over into the nonwettable regions. Liquid spillover is, however, expected to occur [4] once the substrate is sufficiently cooled such that the apparent contact angle exceeds 30°, the advancing wetting contact angle of a macroscopic ethanol drop on a methyl terminated surface. This regime is difficult to obtain experimentally.

By solving numerically Eq. (1) with fixed $\Delta\mu^*$ and different values of w it was also possible to compare the theoretical scaling law for the liquid adsorption onto the stripes to the experimental data of Fig. 3. The theory (solid curves in Fig. 3) again describes well the liquid adsorption on the nanostripes; in particular, it is apparent that in the under-saturated case ($\Delta T = 3, 0.5\,^{\circ}\mathrm{C}$) h is independent of w simply because $h \ll w$ and therefore the liquid stripes behave as if they were an infinitely wide liquid film on a COOH surface. At saturation, Eq. (1) can be approximated as $\gamma \partial^2 l/\partial x^2 \simeq -2A/l^3$, the solution to which gives the predicted $h \sim w^{1/2}$ dependence. This behavior is in good agreement with our measurements and the $\frac{1}{2}$ power law exponent supports the expected dispersive, nonretarded interactions [3]. The thicknesses at saturation are <5 nm which is within the nonretardation regime. In the over-saturated case ($\Delta T = -10\,^{\circ}\mathrm{C}$) the measured behavior is well described by theory with $\Delta\mu^* = -0.6 \times 10^{-4}$. The power law exponent (~2) observed in the limit of large w (>200 nm) follows the predicted dependence for drops with a perfectly circular cross section. This simply indicates that when the liquid thickness is larger than ~8 nm, dispersive forces become less important and the droplet profile is reasonably well described by the macroscopic Young-Laplace equation.

Our experimental results clearly show that condensed nanoliquids can be controlled through the vapor phase and that their shape can be measured *in situ* by using noninvasive, scanning probe techniques. The detailed observations show that the topology of liquid nanostripes is very well described by the augmented Young equation together with an interface potential obtained from DFT assuming dispersive molecular interactions. Specifically, at saturation the profile shapes of the liquid ethanol and their $w^{1/2}$ height dependence are in excellent agreement with the predictions. Although the profile shapes are also well described by the theory away from saturation, the relationship between the theoretical $\Delta\mu$ and ΔT does not follow the expected bulk dependence. Despite this, all profiles at the same ΔT can be described by a single choice of $\Delta\mu$.

This work is supported by the Nanoscale Science, Engineering and Technology Program of the U.S. DOE under Contract No. DE-AC02-98CH10886. B. O. gratefully thanks the Stony Brook University Physics Department for their hospitality. We thank G. McKinley, J. Sagiv, S. Dietrich, and D. Quéré for stimulating discussions.

*Electronic address: ocko@bnl.gov

[1] P. G. de Gennes, F. Brochard-Wyart, and D. Quere, *Capillarity and Wetting Phenomena: Drops, Bubbles, Pearls, Waves* (Springer, New York, 2003).
[2] P. G. de Gennes, Rev. Mod. Phys. **57**, 827 (1985).
[3] C. Bauer and S. Dietrich, Phys. Rev. E **60**, 6919 (1999).
[4] P. Lenz and R. Lipowsky, Phys. Rev. Lett. **80**, 1920 (1998).
[5] R. Maoz, S. Cohen, and J. Sagiv, Adv. Mater. **11**, 55 (1999), and references therein.
[6] I. M. Tidswell, B. M. Ocko, P. S. Pershan, S. R. Wasserman, G. M. Whitesides, and J. D. Axe, Phys. Rev. B **41**, 1111 (1990).
[7] A. Checco, Y. Cai, O. Gang, and B. M. Ocko (to be published).
[8] A. Noy, C. Sanders, D. Vezenov, S. Wong, and C. Lieber, Langmuir **14**, 1508 (1998).
[9] D. Wouters, R. Willems, S. Hoeppener, C. F. J. Flipse, and U. S. Schubert, Adv. Funct. Mater. **15**, 938 (2005).
[10] R. Garcia and R. Perez, Surf. Sci. Rep. **47**, 197 (2002).
[11] A. Checco, J. Daillant, and P. Guenoun, Phys. Rev. Lett. **91**, 186101 (2003).
[12] J. Tamayo and R. Garcia, Langmuir **12**, 4430 (1996).
[13] T. Pompe and S. Herminghaus, Phys. Rev. Lett. **85**, 1930 (2000).
[14] F. Rieutord and M. Salmeron, J. Phys. Chem. B **102**, 3941 (1998).
[15] J. N. Israelachvili, *Intermolecular and Surface Forces* (Academic Press, New York, 1992).
[16] M. Kagan, W. Pinczewski, and P. Oren, J. Colloid Interface Sci. **170**, 426 (1995).
[17] C. Bauer and S. Dietrich, Eur. Phys. J. B **10**, 767 (1999).
[18] T. Ederth, Langmuir **17**, 3329 (2001).
[19] I. Tidswell, T. Rabedeau, P. Pershan, and S. Kosowsky, Phys. Rev. Lett. **66**, 2108 (1991).
[20] M. Robbins, D. Andelman, and J.-F. Joanny, Phys. Rev. A **43**, 4344 (1991).